

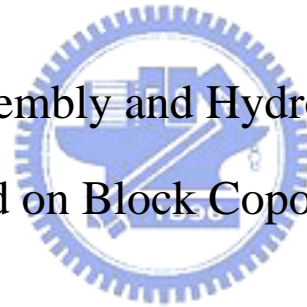
國立交通大學

應用化學研究所

博士論文

團聯式共聚高分子其自組裝與氫鍵作用力之研究

The Study on Self-Assembly and Hydrogen Bonded Interaction
Based on Block Copolymers



研究生：林振隆

指導教授：張豐志 教授

中華民國九十四年九月

團聯式共聚高分子其自組裝與氫鍵作用力之研究

The Study on Self-Assembly and Hydrogen Bonded Interaction Based on
Block Copolymers

研 究 生：林振隆

Student : Chen-Lung Lin

指 導 教 授：張豐志

Advisor : Feng-Chih Chang



A Dissertation
Submitted to Department of Applied Chemistry
College of Science
National Chiao Tung University
in partial Fulfillment of the Requirements
for the Degree of Philosophy
Doctor
in
Applied Chemistry

September 2005

Hsinchu, Taiwan, Republic of China

中華民國九十四年九月


團聯式共聚高分子其自組裝與氫鍵 作用力之研究

學生：林振隆

指導教授：張豐志

國立交通大學應用化學研究所 博士班

摘 要



現今大多數的材料都需要經過額外化學的處理或經由電漿(plasma)改質、塗佈(coating)、表面接枝...等方法才可使材料更適合的運用在特殊領域中，然而經由分子設計過後的團聯式共聚高分子(diblock copolymer)，可以利用許多方法使其自組裝(self-assembly)形成某特殊型態結構，而可應用於特殊功能、材料上之，可省去許多繁雜的改質步驟或費時的額外處理的功夫。因此運用分子設計，而具有自組裝特性的團聯式共聚高分子已受到許多的矚目與探討。

本研究首先分別利用原子轉移自由基聚合反應(atom transfer radical polymerization, ATRP)與縮合反應合成poly(phenylquinoline)- block - poly(methyl methacrylate) (PPQ -*b*-PMMA) 硬-軟鏈段團聯式共聚高分子；之後，將合成出的硬段-軟段段團聯式共聚高分子溶於適當的溶劑中，在具有水氣及風速一定的環境中製備出高規則蜂窩狀、六角柱的多孔性薄膜，並以偏光顯微鏡(OM)及掃描式電子顯微鏡(SEM)觀察此高分子薄膜。此外，並探討此共聚高分子在不同條件下的型態學與孔洞大小、壁厚的趨勢，結果已可成功的控制此高規則多孔性高

子薄膜的孔洞大小。

在 高 分 子 相 關 研 究 領 域 中 ， 高 分 子 聚 摻 一 直 是 個 被 廣 泛 研 究 的 課 題 ， 由 於 高 分 子 摻 混 時 ， 整 個 系 統 會 產 生 很 低 的 熵 (entropy) 值 ， 使 的 絕 大 部 分 的 摻 合 系 統 有 著 很 差 的 相 溶 性 。 透 過 引 入 高 分 子 間 的 特 殊 作 用 力 ， 會 使 得 高 分 子 摻 合 系 統 相 溶 性 顯 著 的 提 升 ， 其 中 ， 又 以 氫 鍵 作 用 力 被 應 用 的 最 廣 泛 。

在 具 有 氫 鍵 作 用 力 的 高 分 子 摻 合 系 統 中 ， 有 各 種 的 理 論 去 描 述 系 統 中 的 作 用 力 行 為 及 相 溶 性 相 圖 ， 其 中 ， 以 Painter-Coleman association model (PCAM) 最 能 準 確 的 闡 述 高 分 子 氫 鍵 摻 合 系 統 。 因 此 ， 在 本 研 究 中 ， 我 們 合 成 出 軟 段 - 軟 段 團 聯 式 共 聚 高 分 子 ， 探 討 由 Painter 及 Coleman 等 人 所 提 出 的 分 子 內 屏 幕 效 應 (intramolecular screening effect) ， 所 導 致 不 同 序 列 分 佈 的 高 分 子 ， 摻 合 時 產 生 的 不 同 氫 鍵 作 用 情 形 。 接 著 再 將 此 團 聯 式 共 聚 高 分 子 摻 混 另 一 種 具 有 不 同 氫 鍵 受 體 (acceptor) 的 高 分 子 ， 進 而 探 討 不 同 序 列 分 佈 對 三 相 氫 鍵 混 摻 系 統 所 造 成 的 不 同 相 溶 情 形 。 此 外 ， 我 們 也 探 討 在 三 相 氫 鍵 混 摻 系 統 中 ， 三 個 皆 具 有 氫 鍵 予 體 (donor) 的 高 分 子 ， 摻 混 時 所 產 生 的 特 殊 完 全 互 溶 型 態 。

The Study on Self-Assembly and Hydrogen Bonded Interaction Based on Block Copolymers

Student : Chen-Lung Lin

Advisors : Dr. Feng-Chih Chang

Institute of Applied Chemistry

National Chiao Tung University



Most of today's materials require additional processing or modification steps in order to obtain the properties that make them suitable for a particular application. As an alternative to these traditional fabrication pathways, routes that use the self-assembly of polymeric building blocks are attracting increasing attention.

We have synthesized rod-coil diblock PPQ-b-PMMA copolymers by using the versatile atom-transfer radical polymerization method and have characterized them by differential scanning calorimetry (DSC), Fourier transform infrared spectroscopy (FTIR), and thermogravimetric analysis (TGA). A regularly porous, honeycomb-structured film was prepared from the dichloromethane solution of the diblock copolymers under a flow of moist air. The diameters of the spherical pores can be controlled in the range from 0.8 to 3 μm by modifying both the rod-coil

copolymers' relative molecular weights and the casting conditions. The wall thickness of the film is varied linearly with the relative molecular mass (M_r).

The miscibility and specific interaction in polymer blends have been a topic of intense interest in polymer science. The miscibility of an immiscible blend was enhanced by introducing one component which can form hydrogen bonded with another component. It is the one of the major achievements during last twenty years in polymer blend. This type of interaction has been widely described in terms of Painter & Coleman association model due to exactly prediction in most systems.

A series of poly(vinylphenol-*co*-methyl methacrylate) (PVPh-*co*-PMMA) block and random copolymers were prepared through anionic and free radical polymerizations, respectively, of 4-*tert*-butoxystyrene and methyl methacrylate and subsequent selective hydrolysis of the 4-*tert*-butoxystyrene protective groups. Analysis of infrared spectra suggests that the random copolymer possesses a higher fraction of hydrogen-bonded carbonyl groups and a larger interassociation equilibrium constant relative to those of a block copolymer containing similar vinylphenol content because of the different sequence distribution that may arise from the so-called intramolecular screening effect. Furthermore, the ternary polymer blend of PVPh, PMMA, and PEO with different sequence distribution was performed to study the phase behavior. The miscibility and hydrogen bonding behavior of ternary hydrogen bonded blend of phenolic/phenoxy/PVPh was also investigated. According to the DSC analysis, every composition of the ternary blend shows single glass transition temperature (T_g), indicating that this ternary hydrogen bonded blend is totally miscible in the amorphous phase.

Acknowledgment

自86年來交大至今，經過八個年頭，這些年來的磨練，讓我成長不少。大學時，多樣的課外活動，從參加到領導，從自我行事到學會團體合作，有歡笑有淚水，這許多的種種事讓我原本尖銳的個性磨滑了許多，也體認到社會化的重要。在大學生涯即將結束時，很幸運的到了張豐志老師的實驗室做專題，期間，在老師及郭紹偉學長的指導下，進入了高分子學門，因為如此，之後就跟高分子化學結下了不解之緣，大四甄試上交大應化研究所後，懷抱著對高分子的熱情，很順利的進入了張豐志老師實驗室。在研究所求學時期，非常感謝張老師的提攜以及郭紹偉學長在碩士論文上的教導，可以幸運的以一年的時間得到碩士學位。



碩士畢業後深感自身學習的不足，毅然的繼續留在張老師實驗室裡做研究，這期間，張老師自由的學風讓我可以放手去做自己想做的研究，雖然歷經了不少挫折，但辛苦後的果實是甜美的。能夠順利的在三年後的今天獲得博士學位，最先要感謝張豐志老師的支持，讓我可以自動自發的以積極的態度去面對過程中的種種難題，不畏艱難的去克服它。很謝謝郭紹偉學長在研究過程中的指導，讓我遇到問題時可以快速的解決疑問。還有感謝寶翔及婉君兩位學妹，如果沒有你們在實驗上的幫忙，我可能無法順利的畢業。感謝同學俊毅、定儒、

忠錫、凱方以及學弟妹家明、欣芳、師吉，在研究上的互相砥礪，因為有你們讓我可以心情不好時，有喝酒解悶的對象，高興時可以盡情的歡笑。感謝已畢業的智峰、文億、一哲學長，在我剛進博士班時的照顧，讓我可以很快的適應，調整心態去面對挑戰。感謝英傑學弟，因為有你讓我的養魚之路不孤單。其他實驗室的學弟妹們，非常感謝大家的幫忙，讓我不管在研究或是課業上可以順利的進行。

最感謝的還有女友佩君，這幾年來，有妳的陪伴，傷心、挫折、失落時，有妳訴苦、解憂，伴我渡過難熬的日子，妳帶給我的歡笑快樂，未來我會努力給妳雙倍的幸福。最後，謝謝我的家人，爸、媽、三位大姊、小弟，有你們的支持，做我最堅強的後盾，我才得以專心的在外地努力，僅以此論文獻給所有曾經幫助過我的人，未來的日子，我會持續努力，盡最大的努力回報大家。

Outline of Contents

| | Pages |
|--|-------|
| Abstract (in Chinese) | I |
| Abstract (in English) | III |
| Acknowledgment | V |
| Out of Contents | VII |
| List of Tables | XI |
| List of Scheme | XIII |
| List of Figures | XIV |
| Chapter 1 Introduction to Supramolecular Materials via Block copolymer | |
| 1-1 Supramolecular Materials from Block Copolymers | 1 |
| 1-2 Coil-Coil Diblock Copolymers | 2 |
| 1-3 Rod-Coil Block Copolymer | |
| 1-3.1 Rod-Coil Block Copolymer Theories | 6 |
| 1-3.2 Rod-Coil Copolymers Based on Helical Rods | 10 |
| 1-3.3 Rod-Coil Copolymers Based on Mesogenic Rods | 11 |
| 1-3.4 Rod-Coil Copolymers Based on Conjugated Rods | 13 |
| 1-4 Introduction to the Honeycomb Morphology and the “breath figures” Method | 15 |
| References | 18 |
| Chapter 2 Introduction to Hydrogen Bonds in Polymer Blends | |
| 2-1 Polymer Blend | 30 |
| 2-2 Introduction to Painter-Coleman Association Model | 31 |
| 2-3 Intramolecular Screening and Functional Group Accessibility Effects in Polymer Blends | 33 |
| 2-4 Ternary Polymer Blends | 40 |
| References | 45 |
| Chapter 3 Synthesis of Rod-Coil Diblock Copolymers by ATRP and their Honeycomb Morphologies formed by the “Breath Figures” Method | |
| Abstract | 49 |
| 3-1 Introduction | 50 |
| 3-2 Experimental Section | |
| 3-2.1 Materials | 52 |

| | |
|---|----|
| 3-2.2 Synthesis of <i>N</i> -(4-acetylphenyl)-2-bromo-2-methylpropanamide | 52 |
| 3-2.3 Polymerization of methyl ketone-terminated poly(methyl methacrylate) | 52 |
| 3-2.4 Synthesis of poly(phenylquinoline)- <i>block</i> -poly(methyl methacrylate) diblock copolymer | 53 |
| 3-2.5 Measurements | 53 |
| 3-3 Results and Discussion | |
| 3-3.1 Synthesis of methyl ketone-terminated PMMA and rod – coil diblock polymers | 55 |
| 3-3.2 Micro-porous honeycomb morphology | 59 |
| 3-4 Conclusions | 62 |
| References | 63 |
| Chapter 4 Sequence Distribution and Polydispersity Index Affect the Hydrogen Bonding Strength of Poly (vinylphenol-co-methyl methacrylate) Copolymers | |
| Abstract | 79 |
| 4-1 Introduction | 80 |
| 4-2 Experimental Section | |
| 4-2.1 Materials | 83 |
| 4-2.2 Synthesis of Poly(vinylphenol- <i>block</i> -methyl methacrylate) by Anionic Polymerization | 83 |
| 4-2.3 Synthesis of Poly(vinylphenol - <i>random</i> -methyl methacrylate) by Free Radical Polymerization | 84 |
| 4-2.4 Blend Preparation | 85 |
| 4-2.5 Measurements | 85 |
| 4-3 Results and Discussion | |
| 4-3.1 Synthesis of poly(vinylphenol- <i>block</i> -methyl methacrylate) copolymer by anionic polymerization | 87 |
| 4-3.2 Synthesis of poly(vinylphenol- <i>random</i> -methyl methacrylate) copolymer through free radical polymerization | 88 |
| 4-3.3 FT-IR analyses | 90 |
| 4-3.4 Thermal Analyses | 96 |

| | | |
|--|---|-----|
| 4-4 | Synthesis of Poly(vinylphenol- <i>block</i> -methyl methacrylate) Copolymer by Atom Transfer Radical Polymerization | |
| 4-4.1 | Materials | 99 |
| 4-4.2 | Preparation of PMMA-Br Macroinitiator | 99 |
| 4-4.3 | Preparation of PAS- <i>b</i> -PMMA by ATRP of 4-acetoxystyrene with PMMA-Br Macroinitiator | 100 |
| 4-4.4 | Deacetylation of Poly(PAS- <i>b</i> -PMMA) | 100 |
| 4-5 | Analysis of PVPh- <i>b</i> -PMMA Copolymer | |
| 4-5.1 | ¹ H NMR Analyses | 100 |
| 4-5.2 | GPC Analyses | 101 |
| 4-5.3 | FT-IR Analyses | 101 |
| 4-5.4 | DSC analysis | 102 |
| 4-6 | Conclusions | 103 |
| | References | 104 |
| Chapter 5 Sequence Distribution Affect the Phase Behavior and Hydrogen Bonding Strength in Blends of Poly(vinylphenol- <i>co</i> -methyl methacrylate) with Poly(ethylene oxide) | | |
| | Abstract | 131 |
| 5-1 | Introduction | 132 |
| 5-2 | Experimental Section | |
| 5-2.1 | Materials | 135 |
| 5-2.2 | Blend Preparation | 135 |
| 5-2.3 | Measurements | 135 |
| 5-3 | Results and Discussion | |
| 5-3.1 | Thermal Analyses | 137 |
| 5-3.2 | FT-IR analyses | 138 |
| 5-4 | Conclusions | 148 |
| | References | 149 |
| Chapter 6 The Totally Miscible in Ternary Hydrogen Bonded Polymer Blend of Poly(vinyl phenol)/Phenoxy/Phenolic | | |
| | Abstract | 171 |
| 6-1 | Introduction | 172 |
| 6-2 | Experimental | |

| | |
|--|-----|
| 6-2.1 Materials | 175 |
| 6-2.2 Preparation of Blend Samples | 175 |
| 6-2.3 Differential Scanning Calorimetry (DSC) | 175 |
| 6-2.4 Infrared Spectra | 175 |
| 6-2.5 Optical Microscopy | 176 |
| 6-3 Results and Discussion | |
| 6-3.1 Binary Blend System | 177 |
| 6-3.2 Ternary Blend System | |
| 6-3.2.1 Thermal Analyses | 178 |
| 6-3.2.2 FT-IR Analysis | 178 |
| 6-3.2.3 Inter-association Equilibrium Constant (K_A) | 180 |
| 6-3.2.4 Optical Micrographs Analysis | 183 |
| 6-4 Conclusions | 184 |
| References | 185 |
| Chapter 7 Conclusions | 200 |
| List of Publications | 202 |
| Introduction to Author | 204 |



List of Tables

| | Pages |
|---|-------|
| Table 3-1: Molecular weights and thermal properties of the methyl ketone-terminated PMMA | 66 |
| Table 3-2: Yields of diblock copolymers calculated after solvent extraction. The values of T_g and T_d and the residual weights were measured and calculated from DSC and TGA measurements. | 67 |
| Table 4-1: Characterization of poly(vinylphenol- <i>block</i> -methyl methacrylate) prepared by anionic polymerization. | 107 |
| Table 4-2: Characterization of poly(vinylphenol- <i>random</i> -methyl methacrylate) prepared by free radical polymerization. | 108 |
| Table 4-3: Results of curve-fitting the data for PVPh- <i>co</i> -PMMA and PVPh/PMMA blends at room temperature. | 109 |
| Table 4-4: Summary of the self-association and interassociation parameters of PVPh- <i>co</i> -PMMA copolymer and PVPh/PMMA blend systems | 110 |
| Table 4-5: The values of T_g and T_g breadth obtained from PVPh- <i>co</i> -PMMA copolymer and PVPh/PMMA blend systems | 111 |
| Table 4-6: The values of T_g obtained from the narrow polydispersity of PVPh | 112 |
| Table 4-7: Molecular weight information of polymers | 113 |
| Table 4-8: Characterization of poly(vinylphenol- <i>block</i> -methyl methacrylate) prepared by ATRP polymerization | 113 |
| Table 5-1: Characterization of PVPh- <i>r</i> -PMMA prepared by free radical polymerization and PVPh- <i>b</i> -PMMA synthesized by anionic polymerization | 152 |
| Table 5-2: Thermal properties of PVPh- <i>r</i> -PMMA/PEO blends | 153 |
| Table 5-3: Thermal properties of PVPh- <i>b</i> -PMMA/PEO blends | 154 |
| Table 5-4: Results of curve-fitting the data for PVPh- <i>r</i> -PMMA and PVPh- <i>r</i> -PMMA/PEO blends at room temperature | 155 |
| Table 5-5: Results of curve-fitting the data for PVPh- <i>b</i> -PMMA and PVPh- <i>b</i> -PMMA/PEO blends at room temperature | 156 |
| Table 5-6: Summary of the self-association and interassociation parameters of PVPh- <i>co</i> -PMMA copolymers and PVPh- <i>co</i> -PMMA/PEO blends | 157 |

| | |
|--|-----|
| Table 5-7: Thermal properties of PVPh/PMMA/PEO ternary polymer blends | 158 |
| Table 6-1: Summary molecular structure, characteristic, T_g , and model compound of polymers used in this study. | 187 |
| Table 6-2: The various association equilibrium constants and thermodynamic parameters were used in this research. | 188 |
| Table 6-3: The fraction of free hydroxyl groups of 4-ethyl phenol | 189 |



List of Scheme

| | Pages |
|------------|-------|
| Scheme 1-1 | 21 |
| Scheme 1-2 | 22 |
| Scheme 1-3 | 22 |
| Scheme 3-1 | 68 |
| Scheme 3-2 | 68 |
| Scheme 3-3 | 69 |
| Scheme 4-1 | 114 |
| Scheme 4-2 | 115 |
| Scheme 4-3 | 116 |



List of Figures

| | Pages |
|---|-------|
| Figure 1-1: Experimental phase diagram for polystyrene- <i>b</i> -polyisoprene diblock copolymers. | 23 |
| Figure 1-2: Theoretical phase diagram for a diblock copolymer near the ODT. | 23 |
| Figure 1-3: Transmission electron micrograph of a blend containing 75 wt.-% of a polystyrene- <i>b</i> -polybutadiene- <i>b</i> -poly(<i>tert</i> -butyl methacrylate) (SBT) triblock copolymer and 25 wt.-% of a polystyrene- <i>b</i> -poly(<i>tert</i> -butyl methacrylate) (st) diblock copolymer. The non-centrosymmetric supramolecular structure of this blend is schematically illustrated in the diagram that assigns the different phases observed in the marked part of the micrograph. | 24 |
| Figure 1-4: Transmission electron micrographs of (a) polyisoprene- <i>b</i> -polystyrene- <i>b</i> -polyvinylpyridine. (From Ref. 13) (b) Axial TEM projection of hexagonally packed structural units. The darkest regions correspond to the OsO ₄ -stained PI domains, while the gray regions are CH ₃ I-stained P2VP domains. | 24 |
| Figure 1-5: Schematic representation of a monolayer puck. | 25 |
| Figure 1-6: Phase diagram including the hockey puck and lamellae phases. The phases are (I) bilayer lamellae, (II) monolayer lamellae, (III) bilayer hockey pucks, (IV) monolayer hockey pucks, and (V) incomplete monolayer lamellae. $\text{Log}(v^3\chi_s)$ is plotted against λ . $\lambda = \phi/(1-\phi)$ where ϕ is the volume fraction of the coil. $v = \kappa/\lambda$ and $\kappa = Na^2/L^2$ where the coil part is assumed to consist of N segments with a mean-square separation between adjacent segments of $6a^2$, and L is the rod length. χ is the Flory-Huggins interaction parameter. | 25 |
| Figure 1-7: Packing model for the formation of “double-hexagonal” organization. | 26 |
| Figure 1-8: (a) TEM image. (b) Schematic packing structure of rod-coil copolymer. | 26 |
| Figure 1-9: (a) Schematic molecular arrangement of three head-to-tail PPE- <i>block</i> -PDMS. (b) Schematic representation of the ribbonlike | 27 |

supramolecular structure formed by PPE-*block*-PDMS.

Figure 1-10: Optical (A to C) and scanning electron (D) micrographs of the typical morphologies of PPQ₅₀-PS₃₀₀. Drops of dilute solutions (0.5 to 1.0 mg/ml) of the diblock copolymers were spread and dried on glass slides and aluminum substrates, respectively. (A) Spherical aggregates (1:1 TFA:DCM, v/v, 95 °C); (B) lamellae (1:1 TFA:DCM, 25 °C); (C) cylinders (9 :1 TFA:DCM, 25 °C); and (D) vesicles (1:1–1:4 TFA:DCM, 25 °C). 27

Figure 1-11: (a) Schematic representation of hierarchical self-organization of PPQ-*b*-PS into ordered microporous structure. (b) Fluorescence photomicrograph of solution-cast micellar film of PPQ_{*m*}-*b*-PS_{*n*} with *m* =10 and *n* = 300. 28

Figure 1-12: A model for the formation of the structure in polymer films. 29

Figure 2-1: Theoretical spinodal phase diagrams for PVPh/EVA[70] blends. Top: Calculated from the derivatives of Eq. 3 containing the “correct” excess free entropy term Eq. 5. Bottom: The same calculation, but with the modified excess free entropy term Eq. 6. 46

Figure 2-2: Theoretical miscibility maps calculated at 25 °C for STVPh/EVA blends. Top: Calculated from the derivatives of Eq. 3 containing the “correct” excess free entropy term Eq. 5. Bottom: The same calculation, but with the modified excess free entropy term Eq. 6. The areas encompassed by the small black dots denote predicted two phase regions. Experimentally determined single and two phase blends are denoted by the unshaded and black filled large circles, respectively. 47

Figure 2-3: Equilibrium constant values for the PVPh-PVAc blend system (FGA: functional group accessibility). 48

Figure 2-4: Calculated fraction of hydrogen bonded acetoxy carbonyl groups for the PVPh-PVAc blend system at 25 °C. 49

Figure 3-1: DSC scans of PMMAs having various degrees of polymerization 70

Figure 3-2: Infrared absorbances of PMMAs having different tacticities. The curve having the solid line represents the syndiotactic-like methyl ketone-terminated PMMA; the dashed line represents that of the isotactic-like PMMA. (The isotactic-like PMMA was synthesized in our 71

| | |
|--|-----|
| laboratory through the use of a different initiator for ATRP.) | |
| Figure 3-3: ^1H NMR spectrum of the PMMA_{1300} . | 72 |
| Figure 3-4: TGA thermograms of PPQ, methyl ketone-terminated PMMA, and rod – coil diblock copolymers under a flow of N_2 at $20\text{ }^\circ\text{C}/\text{min}$. | 73 |
| Figure 3-5: FTIR spectra of methyl ketone-terminated PMMA, the PPQ homopolymer, and the rod – coil diblock copolymer. The arrows indicate the characteristic absorption peaks of the diblock copolymer. | 74 |
| Figure 3-6: POM images prepared by dichloromethane solution of $\text{PPQ}_{52}\text{PMMA}_{2500}$ at concentration of 0.5 wt% under humidity of 73 %. | 75 |
| Figure 3-7: SEM images prepared when using dichloromethane solutions of $\text{PPQ}_{52}\text{PMMA}_{2500}$ at different concentrations. (a) 0.1 wt%; (b) 0.5 wt%; (c) 1 wt%; (d) 0.005 wt%. | 76 |
| Figure 3-8: SEM images prepared when using the same concentration (1 wt%) of different diblock copolymers. (a) $\text{PPQ}_{48}\text{PMMA}_{1300}$; (b) $\text{PPQ}_{52}\text{PMMA}_{2500}$; (c) $\text{PPQ}_{50}\text{PMMA}_{800}$. | 77 |
| Figure 3-9: The plot of pore size and wall thickness versus relative molecular mass (M_r) at constant polymer concentration of 1 wt%. Only five ratios are plotted, because the solubility of $\text{PPQ}_{120}\text{PMMA}_{800}$ is too poor to form the regular porous film. | 78 |
| Figure 4-1: GPC traces of PVPh- <i>b</i> -PMMA block copolymers. (a) First block poly(<i>tert</i> -butoxystyrene) (<i>Pt</i> BOS), $M_n = 8000\text{ g/mol}$, $\text{PDI} = 1.08$; (b) poly(vinylphenol- <i>b</i> -methyl methacrylate) (PVPh- <i>b</i> -PMMA), $M_n = 16000\text{ g/mol}$, $\text{PDI} = 1.11$. | 117 |
| Figure 4-2: ^1H NMR spectra of (a) before hydrolysis, <i>Pt</i> BOS- <i>b</i> -PMMA, and (b) after hydrolysis, PVPh- <i>b</i> -PMMA. | 118 |
| Figure 4-3: ^{13}C NMR spectra of (a) before hydrolysis, <i>Pt</i> BOS- <i>b</i> -PMMA, and (b) after hydrolysis, PVPh- <i>b</i> -PMMA. | 119 |
| Figure 4-4: IR spectra of (a) pure PVPh, (b) <i>Pt</i> BOS- <i>b</i> -PMMA, (c) PVPh- <i>b</i> -PMMA, and (d) pure PMMA at room temperature ranging from $400 - 4000\text{ cm}^{-1}$. | 120 |
| Figure 4-5: Kelen-Tüdös plot for the <i>Pt</i> BOS- <i>r</i> -PMMA copolymers. | 121 |
| Figure 4-6: FT-IR spectra in the $2700 - 3800\text{ cm}^{-1}$ region for (a) random copolymer, (b) block copolymer, and (c) polymer blend. | 122 |

| | |
|--|-----|
| Figure 4-7: Comparison between the FTIR spectra (2700–3800 cm^{-1}) of samples having similar PVPh contents. | 123 |
| Figure 4-8: FT-IR spectra (1670 – 1760 cm^{-1}) of a (a) random copolymer, (b) block copolymer, and (c) polymer blend. | 124 |
| Figure 4-9: Plots of the fraction of hydrogen-bonded carbonyl groups vs. the PVPh fraction for a random, block copolymer, and polymer blend. | 125 |
| Figure 4-10: DSC traces of (a) PVPh- <i>r</i> -PMMA copolymers, (b) PVPh- <i>b</i> -PMMA copolymers and (c) PVPh/PMMA blend. | 126 |
| Figure 4-11: Plots of T_g vs, composition based on (symbol) experimental data. | 127 |
| Figure 4-12: ^1H NMR spectra of (a) PMMA (d_6 -DMSO), (b) PAS- <i>b</i> -PMMA (CDCl_3), and (c) PVPh- <i>b</i> -PMMA (d_6 -DMSO). | 128 |
| Figure 4-13: FT-IR spectra of (a) PMMA, (b) PMMA- <i>b</i> -PAS, and (c) PMMA- <i>b</i> -PVPh recorded at room temperature between 600-4000 cm^{-1} . | 129 |
| Figure 4-14: DSC traces of PVPh- <i>b</i> -PMMA copolymers through ATRP. | 130 |
| Figure 5-1: DSC thermograms of PVPh- <i>r</i> -PMMA/PEO blends having different compositions for (A) 92- <i>r</i> -8/PEO, (B) 76- <i>r</i> -24/PEO, (C) 58- <i>r</i> -42/PEO, and (D) 30- <i>r</i> -70/PEO. | 159 |
| Figure 5-2: Plots of T_g vs weight of PEO for the copolymer/PEO: (A) PVPh- <i>r</i> -PMMA/PEO and (B) PVPh- <i>b</i> -PMMA/PEO blends. | 160 |
| Figure 5-3: DSC thermograms of PVPh- <i>b</i> -PMMA/PEO blends having different compositions for (A) 75- <i>b</i> -25/PEO, (B) 55- <i>b</i> -45/PEO, (C) 40- <i>b</i> -60/PEO, and (D) 30- <i>b</i> -70/PEO. | 161 |
| Figure 5-4: FTIR spectra in the 3050 – 3750 cm^{-1} region for (A) 92- <i>r</i> -8/PEO and (B) 30- <i>r</i> -70/PEO. | 162 |
| Figure 5-5: FTIR spectra in the 3050 – 3750 cm^{-1} region for (A) 75- <i>b</i> -25/PEO and (B) 30- <i>b</i> -70/PEO. | 163 |
| Figure 5-6: Plots of $\Delta\nu$ vs weight of PEO for the copolymer/PEO: (A) PVPh- <i>r</i> -PMMA/PEO and (B) PVPh- <i>b</i> -PMMA/PEO blends. | 164 |
| Figure 5-7: FTIR spectra in the 1320 – 1380 cm^{-1} region for (A) 92- <i>r</i> -8/PEO and (B) 30- <i>r</i> -70/PEO. | 165 |
| Figure 5-8: FTIR spectra in the 1320 – 1380 cm^{-1} region for (A) 75- <i>b</i> -25/PEO and (B) 30- <i>b</i> -70/PEO. | 166 |
| Figure 5-9: FTIR spectra (1670 – 1780 cm^{-1}) of a (A) 92- <i>r</i> -8/PEO and (B) | 167 |

- 30-*r*-70/PEO.
- Figure 5-10: FTIR spectra ($1670 - 1780 \text{ cm}^{-1}$) of a (A) 75-*b*-25/PEO and (B) 30-*b*-70/PEO. 168
- Figure 5-11: Plot of the calculated (—) and experimental (■) values of the fraction of hydrogen bonded carbonyl groups in blends of (A) PVPh-*r*-PMMA/PEO and (B) PVPh-*b*-PMMA/PEO blends where the volume fraction of PEO was hold at 0.2. 169
- Figure 5-12: Ternary phase diagram of (A) PVPh-*r*-PMMA/PEO and (B) PVPh-*b*-PMMA/PEO blends. The open circles represent a miscible ternary blend, and the full circles represent an immiscible ternary blend. 170
- Figure 6-1: DSC traces of the individual binary blends (wt/wt %) having varying compositions: (a) phenolic/PVPh, (b) phenolic/phenoxy, (c) phenoxy/PVPh. 190
- Figure 6-2: Plots of T_g versus the composition of the individual binary blend: (a) phenolic/PVPh, (b) phenolic/phenoxy, (c) phenoxy/PVPh. 191
- Figure 6-3: DSC thermograms of phenolic/phenoxy/PVPh blends of different compositions. (a) 10/36/54 (wt/wt/wt %); (b) 10/35/35; (c) 10/72/18; (d) 30/14/56; (e) 30/35/35; (f) 30/56/14; (g) 50/20/30 (h) 50/40/10; (i) 65/21/14; (j) 80/4/16; (k) 80/10/10; (l) 80/16/4. 192
- Figure 6-4: Ternary phase diagram of the phenolic/phenoxy/PVPh system with individual values of T_g indicated for the composition shown in each cycle. 193
- Figure 6-5: Scatter plots of the values of T_g based on experimental data (●) and the solid line calculated using the Fox equation. 194
- Figure 6-6: Infrared spectra recorded in the region $2700-3700 \text{ cm}^{-1}$ for a series of phenolic/phenoxy/PVPh compositions: (a) 0/0/100 (wt/wt/wt %); (b) 0/100/0; (c) 100/0/0; (d) 50/40/10; (e) 50/30/20; (f) 50/25/25; (g) 50/20/40; (h) 50/10/40. 195
- Figure 6-7: Infrared spectra recorded at room temperature in the region from $3100-3700 \text{ cm}^{-1}$. 196
- Figure 6-8: The absorption band of the free hydroxyl group of 4-ethylphenol (0.02 mol/L) in EPH/2,4-xylenol/cyclohexane solutions, ranging from $3100-3700 \text{ cm}^{-1}$. 197

Figure 6-9: Scale-expanded infrared spectra ranging from 3100-3700 cm^{-1} . 198

Figure 6-10: Optical micrographs of phenolic/phenoxy/PVPh blends of various compositions and at different temperatures. (a) 30/14/56, 100 °C; (b) 30/14/56, 190 °C; (c) 65/17.5/17.5, 100 °C; (d) 65/17.5/17.5, 190 °C. 199

